Metastable Filamentary Vortex Flow in Thin Film Superconductors

Niels Grønbech-Jensen, A. R. Bishop, and Daniel Domínguez
Theoretical Division, Los Alamos National Laboratory, Los Alamos, New Mexico 87545
(Received 7 December 1995)

We present simulations of vortex dynamics in amorphous two-dimensional thin film superconductors, using a new exact method to evaluate long-range interactions between vortices. We find that the onset of dissipation for increasing current is dominated by filamentary channels of flow which are stable in a finite range of bias current. This results in novel steps in the differential resistance, which are strongly history dependent. Our results are in good agreement with recent experiments on amorphous $Mo_{77}Ge_{23}$ superconducting thin films. [S0031-9007(96)00030-0]

PACS numbers: 74.60.Ge, 05.40.+j, 74.76.–w

The issues of depinning and nonlinear transport in a driven disordered medium are of great interest in a large variety of systems [1]. The competition between interaction forces and randomness under an external driving force leads to multiple dynamical regimes. In particular, the dynamics of vortices in disordered type-II superconductors driven by an external current has attracted much attention lately. Experiments on 2*H*-$NbSe_2$ [2] obtained a nonequilibrium phase diagram of the dynamical regimes in the current-voltage (*IV*) characteristics. Structural evidence of these regimes was found in neutron scattering measurements [3]. Three distinct regimes as a function of increasing current were observed: (i) no motion, pinned vortices; (ii) disordered, plastic motion; and (iii) coherently moving vortex lattice. However, recent experiments [4] on amorphous $Mo_{77}Ge_{23}$ thin films found a novel dynamical regime at very low temperatures: the onset of voltage shows abrupt steps in the differential resistance and a strong history dependence. Furthermore, experiments [5] on $YBa_2Cu_3O_{7-\delta}$ just below the melting transition temperature revealed a regime between (i) and (ii) with "steps" in the *IV* curve.

It is now well established that the onset of vortex motion takes place through "channels" of plastic vortex flow. Following early work by Brandt [6], Jensen *et al.* [7] performed molecular dynamics (MD) simulations of vortices in two dimensions (2D). They found that for all but very weak pinning, the vortex lattice is plastically deformed and the onset of vortex motion takes place through channels. This result goes beyond the applicability of the collective pinning theory for *IV* characteristics [8]. Further numerical studies of plastic flow and the onset of vortex motion were carried on by several authors [9]. In all the MD simulations [7,9], the onset of plastic vortex flow occurs at a single threshold force (critical current), above which the voltage increases continuously and nonlinearly. This type of behavior was observed in the experiments on 2*H*-$NbSe_2$ [2,3]. Fisher [1] has proposed that the depinning transition should follow a power law $V \sim (I - I_c)^{\zeta}$, a result recently seen in a gauge glass model simulation [10]. The experimental results of Hellerqvist *et al.* [4] in amorphous thin films, however, show a strong history dependence of the threshold force and abrupt rises of the voltage [11]. In this Letter we provide realistic MD simulations of amorphous thin films that reproduce this novel dynamical regime. Some of our results are also relevant to the experiment in Ref. [5].

The MD simulations of [6,7,9] are in 2D systems with *short-range* vortex-vortex interactions. A short-range 2D potential corresponds to the interactions of 3D vortices considered as rigid rods, where the interaction range is given by the magnetic penetration depth λ. This is correct for thick films where the sample thickness is $d \gg \lambda$ but much smaller than the Larkin-Ovchinikov correlation length [8]. However, in 2D thin films where $d \ll \lambda$ (like the ones of [4]) the vortex-vortex interactions are truly *long range* [12]. Here, we consider the normalized vortex-vortex interaction energy [12],

$$U_{vv}(r_{ij}) = H_0(r_{ij}) - N_0(r_{ij}), \tag{1}$$

where H_0 and N_0 are the Struve and Neumann functions, respectively, and $r_{ij} = |\mathbf{r}_i - \mathbf{r}_j|$ is the normalized two-dimensional distance between the ith and jth vortices. Distance is normalized to the effective 2D penetration depth, $\Lambda = 2\lambda^2/d$, and energy to $E_0 = \Phi_0^2/2\mu_0\Lambda$, with the flux quantum $\Phi_0 = h/2e$. The vortices also interact with impurities (pinning centers). The normalized pinning potential between a vortex and a pinning center is assumed to be [7], $U_{vp}(r) = -A_p e^{-(r/\tilde{a}_p)^2}$, where $\tilde{a}_p$ is the normalized interaction range of the impurity, and A_p is the pinning strength. The normalized equation of motion for the ith vortex is taken as

$$\frac{d\mathbf{r}_i}{dt} = -\sum_{j\neq i} \nabla_i U_{vv}(r_{ij}) - \sum_k \nabla_i U_{vp}(r_{ik}) + \mathbf{F} + \boldsymbol{\eta}_i(t), \tag{2}$$

where $\nabla_i = (\frac{\partial}{\partial x_i}, \frac{\partial}{\partial y_i})$. Time is normalized to $\tau = \Lambda^2\nu/E_0$, where the friction parameter is $\nu = \Phi_0 B d/\rho_f$, the magnetic field perpendicular to the system is B, and the flux flow resistivity is $\rho_f \approx B\rho_n/H_{c2}$. The normalized force on the vortices arises from the applied

current density $\mathbf{J}$, $\mathbf{F} = \mathbf{J} \times \hat{\mathbf{z}}\Phi_0 d\Lambda/E_0$, with $\hat{\mathbf{z}} \parallel \mathbf{B}$. We assume $\mathbf{J} \parallel \hat{\mathbf{x}}$, and thus, $\mathbf{F} \parallel \hat{\mathbf{y}}$. The voltage response (vortex speed) from the ith vortex is then $V_i = dy_i/dt$ (normalized to $\pi\hbar/\tau e$). Thermal noise is modeled as a Langevin white noise, $\boldsymbol{\eta}(t)$, with $\langle \boldsymbol{\eta}_i(t) \rangle = \vec{0}$ and $\langle \boldsymbol{\eta}_i(t_1) \cdot \boldsymbol{\eta}_j(t_2) \rangle = 4\frac{kT}{E_0}\delta_{ij}\delta(t_1 - t_2)$, and temperature T. The summations over j and k represent the vortex-vortex and vortex-impurity interactions, respectively. A new method to simulate a system with periodic boundary conditions and long-range interactions is used. The interaction between a vortex and all the periodic images of another vortex is evaluated with an exact fast converging sum [13].

To connect our simulations to the experiments of [4] we adopt parameter values appropiate for their sample of amorphous $Mo_{77}Ge_{23}$. The length scales are $\Lambda \approx 198\ \mu$m, the mean intervortex distance $a_0 = (\Phi_0/B)^{1/2} = 1.03 \times 10^{-3}\Lambda$, and the pinning range is taken as the coherence length, $a_p \approx \xi = 2.8 \times 10^{-5}\Lambda$. This places us in the regime $a_p \ll a_0 \ll \Lambda$. The temperature $T = 150$ mK in the experiments gives $kT/E_0 \approx 257 \times 10^{-6}$, and from the flux flow resistance R_f we estimate $\tau \approx 4.8 \times 10^{-4}$ s. From the value of the critical current density, we can estimate the pinning strengh from collective pinning theory [8] $A_p \approx 5 \times 10^{-2}\sqrt{n_v/n_p}$, where $n_v = 1/a_0^2$ and n_p are the densities of vortices and pinning centers, respectively. (Even though collective pinning theory is not fully valid here, we expect that still gives the correct order of magnitude.) There is only one free parameter left, n_p. Since the material is amorphous, $n_p > n_v$ seems reasonable. We take $n_p/n_v = 5$ and we simulate a system of size $L^2 = 0.01 \times 0.01$ [14], giving $N_v = 100$ vortices and $N_p = 500$ pinning centers. The positions of the pinning centers are distributed randomly. Because of the extremely small a_p, a very small time step of the numerical integrator was chosen, $dt \leq 2.5 \times 10^{-8}$. Each simulation was started with a different random initial configuration of the vortex positions. Such a configuration quickly relaxes to a random state resembling a state obtained by decreasing the current from the flux-flow regime. For each value of F (stepped in unit increments), a transient time of $\Delta t_{\rm tr} = 625 \times 10^{-6}$ was allowed before data were obtained over the next time of $\Delta t_{\rm av} = \Delta t_{\rm tr}$. We show results here for the deterministic ($T = 0$) cases only. (Finite T will be discussed elsewhere.)

The depinning process is characterized by a competition between the pinning forces and the vortex lattice elastic properties [8]. For 3D vortex interaction potentials, the shear modulus is given by $C_{66} = B\Phi_0/16\pi\mu_0\lambda^2$, and the compression modulus is $C_{11}(k) = B^2/\mu_0(1 + \lambda^2 k^2)$, with k the wave vector of the elastic deformation [8]. For systems with short-range interactions $k\lambda \ll 1$ and so there is local elasticity since C_{11} is dispersionless. This gives $C_{66}/C_{11} = (a_0/\lambda)^2/16\pi$. In most of the simulations [6,7,9] $\lambda \gtrsim a_0$, so $C_{66} \lesssim C_{11}$. For 2D long-range vortex potentials [Eq. (1)], the shear modulus is the same, $C_{66}d = B\Phi_0/8\pi\mu_0\Lambda$, but the compression modulus is now $C_{11}d = 2B^2/\mu_0 k(1 + \Lambda k)$ [15]. This implies that *in thin films elasticity is nonlocal at all length scales.* Furthermore, the vortex lattice is incompressible since $C_{11}(k \to 0) = \infty$. In thin films Λ is of the order of the sample size ($\Lambda \approx L/2$ in [4]), so for most of the deformations $\Lambda k \gg 1$. This gives $C_{66}/C_{11} = (ka_0)^2/16\pi$; since typically $ka_0 \ll 1$, we have $C_{66} \ll C_{11}$. In contrast to short-range interactions, this provides for relatively easy channeling as the interaction favors an overall uniform density while being largely unaffected by deformations such as filamentary flow. The situation of $C_{66}/C_{11} \propto (ka_0)^2 \ll 1$ can also take place in 3D superconductors close to the melting transition, as in the experiments of Ref. [5]. This is because close to melting, C_{66} is largely reduced from its $T = 0$ value, and the effective $\lambda(T)$ is large. In this 3D case there are also vortex line fluctuations along the $\hat{\mathbf{z}}$ direction.

We now discuss our simulation results. The upper inset of Fig. 1 shows seven *IV* curves obtained for different initial conditions but the same distribution of pinning sites. The voltage $\langle V \rangle$ is the normalized voltage per vortex. The lower inset of Fig. 1 shows the voltage noise strength, $\delta V = \sqrt{\langle V^2 \rangle - \langle V \rangle^2}$. The noise relative to the voltage clearly decreases as the voltage approaches free flux flow.

For small forces there is a pinned vortex state. This is a fixed point of the dynamics of Eq. (2) with $\mathbf{r}_i(t) = \mathbf{r}_i^0$, corresponding to $\partial_{x_i} U\{\mathbf{r}_i^0\} = 0$; $\partial_{y_i} U\{\mathbf{r}_i^0\} = F$, with $U = \sum_{ij} U_{vv}(r_{ij}) + \sum_{ik} U_{vp}(r_{ik})$. Because of the many metastable minima of this strongly disordered system, there are many possible pinned states. By increasing F, the basin of attraction of the less stable fixed points (pinned states) shrinks until they become unstable, sequentially. When the last pinned state becomes unstable the vortices move. This argument leads to a unique, well defined threshold force [1]. However, it is possible to have, for the same F, a coexistence of fixed points (pinned states) and attractors corresponding to moving vortices. In this

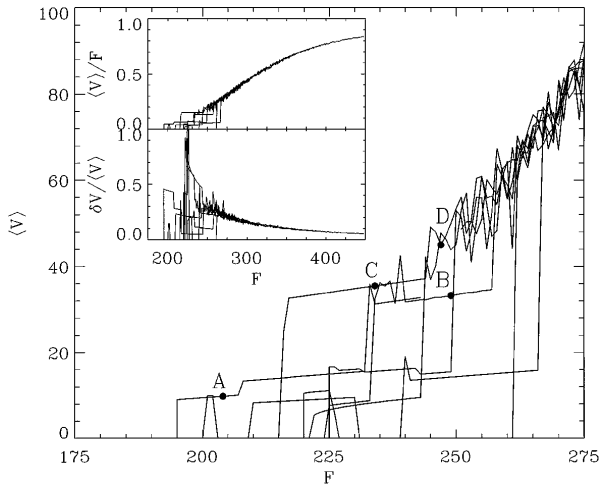

FIG. 1. Simulated *IV* (force-velocity) characteristics for increasing bias current. The insets show the full *IV* curves (upper) and the corresponding noise (lower). The labels A, B, C, D indicate dynamics shown in detail in Fig. 2.

case there is no well defined threshold force and the *IV* curve should be history dependent and hysteretic. Figure 1 indeed shows multiple routes for the onset of voltage, depending on the initial vortex configuration. For each route, there is an abrupt jump to a state with a linear voltage-current dependence with a small slope. At higher currents there are further jumps to other linear voltage regimes. Different routes give a different set of jumps and linear voltage regimes. This behavior closely resembles the experiments on amorphous $Mo_{77}Ge_{23}$ (see Fig. 4 in Ref. [4]).

Figure 2 shows details of the spatiotemporal vortex dynamics for the selected points (A–D) labeled on Fig. 1. Figure 2(a) shows the distribution of vortex velocities (relative to the free flow velocity $V = F$, in normalized units). In this case we observe 11 vortices moving at $\langle V_i \rangle \approx 0.4F$. The left inset shows the traces ($\cdots$) of all the vortices throughout the simulation time ($\Delta t_{\rm av}$) along with a snapshot of positions ($\bullet$). The right inset shows the spectral power of the total normalized voltage $V(t)$. We see that there is a single flow channel, which corresponds to a *one-dimensional* path, i.e., the flow is filamentary. Strikingly, the only effect of increasing F is to increase the speed of the vortices inside the channel, while the structure of the channel and pinned vortices remains stable *in a wide region of* F, resulting in a linear voltage. This filamentary flow state is an attractor where $\mathbf{r}_{i_p}(t) = \mathbf{r}^0_{i_p}$ for the vortices i_p that remain pinned, and $\mathbf{r}_{i_c}(t) = \mathbf{R}(t + t_{i_c})$ for the vortices i_c in the channel. The attractor is periodic, $\mathbf{R}(t + T) = \mathbf{R}(t)$. After a period T all the vortices slip into the positions that were previously occupied by their nearest neighbors. The period and the time delay between the moving vortices are given by the incompressible nature of the vortex system as $T = \langle t_{i_c+1} - t_{i_c} \rangle \approx a_0/v$ with $v = \langle V_i \rangle$. This gives high frequency spectral peaks at multiples of $\omega_0 \approx \frac{2\pi}{a_0}\langle V_i \rangle$ [16]. Replacing this state in (2), we obtain a linear voltage $V = (N_{vc}/N_v)v \approx (N_{vc}/N_v)[F - \frac{1}{N_{vc}}\sum_{i_c}\langle \partial_{y_{ic}} U \rangle]$, with N_{vc} the number of vortices in the channel. When increasing F, at a given moment the channel becomes unstable and the system switches to a different attractor characterized by a new spatiotemporal channel structure, which is again

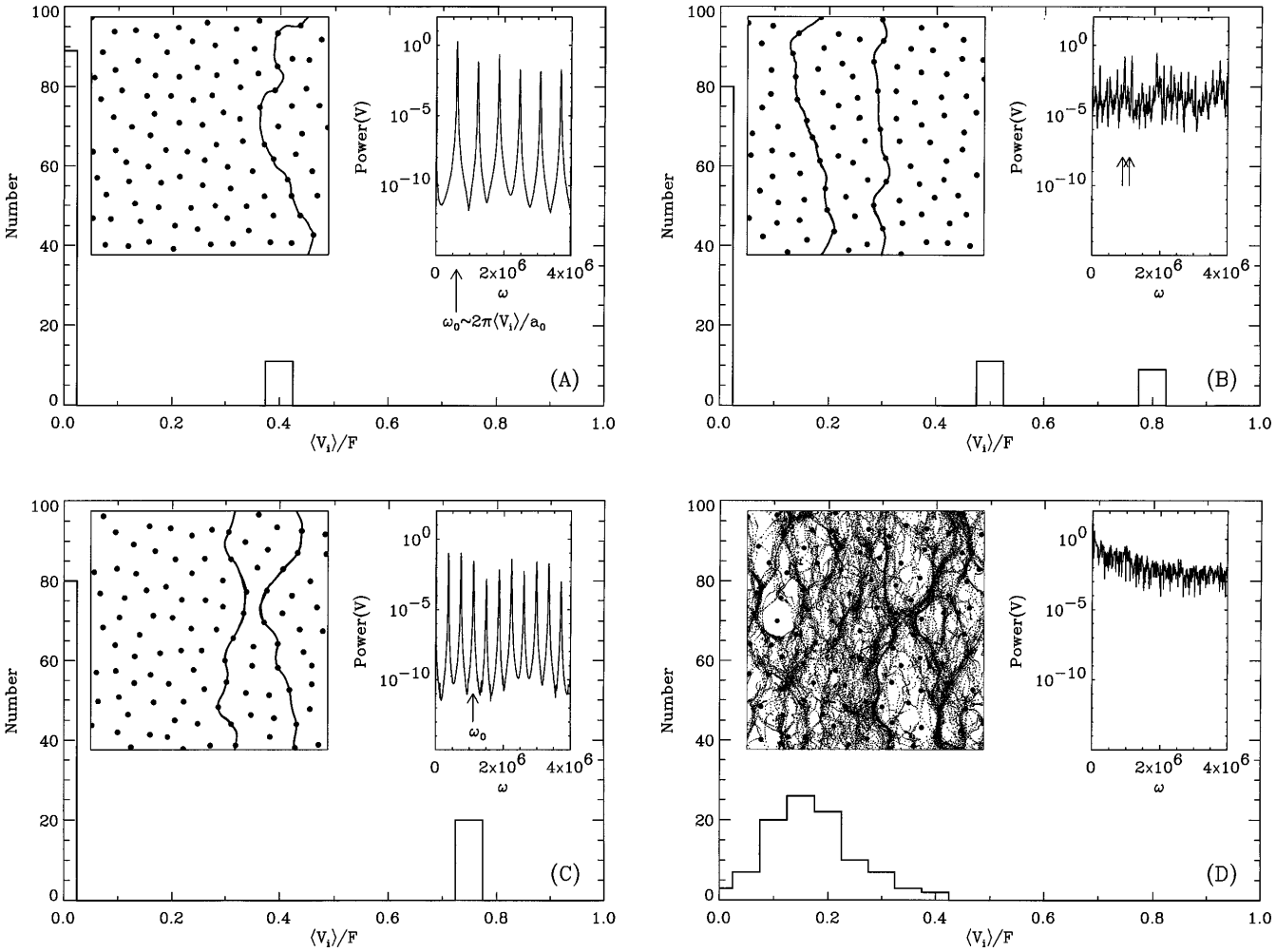

FIG. 2. Details of the dynamical states labeled in Fig. 1. Density of the normalized speed is shown. Insets show (left) the flow traces ($\cdots$) and a snapshot ($\bullet$) of the vortices, and (right) the spectral density of the voltage responses.

stable in a range of F. This results in sudden jumps in the IV curve between different linear regimes. We note that a jump does not necessarily mean that a new channel is opened up over an already existing channel structure, since in general the jumps correspond to switches between different patterns of channel flow. If one assumes that in a large sample there are $n_{\rm ch}$ widely separated channels, each step in the differential resistance is then given by $dV/dI \approx n_{\rm ch}(N_{vc}/N_v)R_f = n_{\rm ch}(a_0/L_y)R_f$. This gives $n_{\rm ch} \approx 180$ for the lowest steps in [4], with a typical distance between channels of $\approx 80a_0$. More complicated dynamics can also occur. For example, we observe filamentary flow where a channel branches into two filaments at a given point and rejoins at a second point [13]. Also multiple channel attractors show more complex dynamics. In Fig. 2(b) we show a double channel dynamical state. One of the channels has 11 vortices with $\langle V_i \rangle \approx 0.5F$, while the other, with 9 vortices, flows at $\langle V_i \rangle \approx 0.8F$. The spectral density response suggests quasiperiodic dynamics: since the two channels are almost uncoupled, each of them has periodic behavior independently [their frequencies are shown in Fig. 2(b)], and then their dynamics is a superposition of two incommensurate periodic responses. A case where two channels interact is shown in Fig. 2(c). Here, a local gear wheel effect synchronizes the flow in the two channels. The average velocity $\langle V_i \rangle \approx 0.75F$ is the same for all vortices since there is an equal number of them in the channels. The synchronization results in periodic flow with subharmonics due to the alternating motion in the two channels. Regardless of the complexity of the filamentary flow, the common feature is that a given channel structure is stable in a wide region of F, giving linear voltages. We have also seen this dynamics for larger samples $L \times L = (0.015)^2, (0.02)^2$ [13].

Figure 2(d) shows the flow pattern *above* the region of filamentary flow. We find a broad distribution of the vortex velocities, indicating a stick-slip type of plastic motion. This is confirmed by the flow pattern which has regions with small but finite activity, and regions with large activity [note that these active regions resemble the well defined channels shown in Figs. 2(a)–2(c)]. A given vortex in this type of flow will show stick-slip behavior, i.e., intermittently participating in efficient channels or being pinned at off-channel sites. The spectral density of the voltage shows broad contributions, indicating that the attractor is chaotic. Finally, at even higher currents all the vortices flow freely in an ordered lattice state [9].

The results shown in this Letter are for increasing F only, where the experiment showed steps in dV/dI at the onset of dissipation. When decreasing F in the simulations from a moving state, we find that the system stays longer in the stick-slip plastic flow state [Fig. 2(d)] but eventually switches down to a single channel at low F [e.g., Fig. 2(a)]. The experiments, however, showed no sign of steps in dV/dI for decreasing currents. A possible reason is that thermal fluctuations may stabilize the chaotic plastic flow state when decreasing the current. Preliminary simulations with $T = 150$ mK show that the system indeed stays longer in the plastic flow state, but still switches to a filamentary flow state at much lower F [13]. Note also that we have the free parameter n_p in our model. Simulations with values of n_p/n_v in the range 1–10 show that filamentary flow occurs over larger current ranges for smaller n_p/n_v.

In conclusion, we have simulated vortex dynamics in a 2D system treating long-range interaction forces exactly. Our simulations compare well with recent experiments on amorphous $Mo_{77}Ge_{23}$ thin films [4]. We reproduce the history dependent structure of sudden jumps and steps in dV/dI observed close to the threshold. These are consequences of the very small shear modulus $C_{66} \ll C_{11}$, the nonlocal elasticity, and the numerous metastable pinned states of this disordered system.

We acknowledge valuable discussions with A. Kapitulnik and L. N. Bulaevskii. This work was performed under the auspices of the U.S. Department of Energy.

[1] See, for example, D. S. Fisher, in *Nonlinearity in Condensed Matter*, edited by A. R. Bishop *et al.* (Springer-Verlag, New York, 1987).
[2] S. Bhattacharya and M. J. Higgins, Phys. Rev. Lett. **70**, 2617 (1993); Phys. Rev. B **49**, 10 005 (1994); A. C. Marley *et al.*, Phys. Rev. Lett. **74**, 3029 (1995); S. Bhattacharya and M. J. Higgins, Phys. Rev. B **52**, 64 (1995).
[3] U. Yaron *et al.*, Nature (London) **376**, 743 (1995).
[4] M. C. Hellerqvist *et al.* (to be published).
[5] G. D' Anna *et al.*, Phys. Rev. Lett. **75**, 3521 (1995).
[6] E. H. Brandt, Phys. Rev. Lett. **50**, 1599 (1983).
[7] H. J. Jensen *et al.*, Phys. Rev. Lett. **60**, 1676 (1988); H. J. Jensen *et al.*, Phys. Rev. B **38**, 9235 (1988); H. J. Jensen *et al.*, J. Low Temp. Phys. **74**, 293 (1989).
[8] A. I. Larkin and Yu. N. Ovchinnikov, J. Low Temp. Phys. **34**, 409 (1979).
[9] A.-C. Shi and A. J. Berlinsky, Phys. Rev. Lett. **67**, 1926 (1991); O. Pla and F. Nori, *ibid.* **67**, 919 (1991); A. E. Koshelev, Physica (Amsterdam) **198C**, 371 (1992); A. E. Koshelev and V. M. Vinokur, Phys. Rev. Lett. **73**, 3580 (1994).
[10] D. Domínguez, Phys. Rev. Lett. **72**, 3096 (1994); D. Domínguez, N. Grønbech-Jensen, and A. R. Bishop (to be published).
[11] Some reproducible structure at the onset of flow was first seen in [2]. However, it consists of jagged peaks in the differential resistance instead of the plateaus seen in [4].
[12] J. Pearl, Appl. Phys. Lett. **5**, 65 (1964).
[13] Details will be published elsewhere.
[14] For $\Lambda \gg L$, studied in this Letter, we are mainly sampling the logarithmic part of the potential (1).
[15] This can be calculated from Eq. (50) in A. L. Fetter and P. C. Hohenberg, Phys. Rev. **159**, 330 (1967).
[16] The period here is very different from the low frequency, size dependent, transit time $\tau_T = L_y/v$, which is sensitive to boundary conditions [5].